Structural transformations and spectroscopic properties of Ni-doped magnesium aluminosilicate glass-ceramics nucleated by a mixture of TiO2 and ZrO2 for broadband near-IR light emission

Aymeric Dugue, Olga Dymshits, Laurent Cormier, Pavel Loiko, Irina Alekseeva, Marina Tsenter, Kirill Bogdanov, Gerard Lelong, Alexander Zhilin

Structural transformations and spectroscopic properties of Ni-doped magnesium aluminosilicate glass-ceramics nucleated by a mixture ofTiO_2 and ZrO_2 for broadband near-IR light emission

Aymeric Dugué[a], Olga Dymshits [b, *], Laurent Cormier [a], Pavel Loiko [c], Irina Alekseeva [b],

Marina Tsenter [b], Kirill Bogdanov [c], Gerard Lelong [a], Alexander Zhilin [b]

[a] *Sorbonne Université, Muséum National d'Histoire Naturelle, UMR CNRS 7590, IRD, Institut de Minéralogie, de Physique des Matériaux et de Cosmochimie,*

IMPMC, 4 Place Jussieu, 75005, Paris, France

[b] *Vavilov State Optical Institute, #36, Babushkina Str., 192171, St. Petersburg, Russia*

[c] *University ITMO, 49 Kronverkskiy Pr., 197101, St. Petersburg, Russia*

ABSTRACT. Ni:$MgAl_2O_4$ spinel shows a reversible random Ni^{2+} site redistribution with increasing temperature. With the aim of determining the influence of the structure evolution induced by heat-treatment on the nature of luminescence centers in NiO-doped spinel-based magnesium aluminosilicate glass-ceramics nucleated by a mixture of TiO_2 and ZrO_2, the detailed spectroscopic study of the initial glass during its heat- treatments at increasing and decreasing temperatures has been performed and accompanied by an XRD analysis and Raman spectroscopy. The initial glass was X-ray amorphous. Its optical spectrum is mainly

formed by absorption of $^{[5]}Ni^{2+}$ sites with a small amount of $^{[4]}Ni^{2+}$ ones. Crystals of the nucleating catalyst, $ZrTiO_4$, about 4 nm in size, appear during heat-treatment at 800 °C, while the absorption spectrum of Ni^{2+} ions remains near unchanged. At 850 °C, spinel crystals with size of about 6 nm precipitate, which is accompanied by a

broadband luminescence in the near-IR centered at 1330 nm with a bandwidth of 380 nm. At 950 °C, there is a slight reduction in intensity of absorption bands attributed to $^{[6]}Ni^{2+}$, which can be explained by a tendency toward random Ni^{2+} site redistribution with increasing temperature. A decrease in the amount of the $^{[6]}Ni^{2+}$ luminescent centers is not accompanied by a decrease in the luminescence intensity because of the increased size of spinel crystals. Additional low-temperature heat-treatment does not lead to a redistribution between $^{[6]}Ni^{2+}$ and $^{[4]}Ni^{2+}$ sites in spinel crystals in favor of $^{[6]}Ni^{2+}$ ones. An increase of the luminescence intensity after low-temperature heat-treatment is associated with additional spinel crystallization.

1. Introduction

Divalent nickel (Ni^{2+}) ions with octahedral symmetry of the ligand field exhibit broadband emission in the near-IR spectral range (1-2 μm) featuring a relatively long luminescence lifetime, which is due to the $^3T_2(^3F) \rightarrow {}^3A_2(^3F)$ transition [1-15] and Refs. therein. Various materials were considered in recent years for Ni^{2+} doping, namely, glasses, transparent glass-ceramics, ceramics and crystals. Luminescent Ni^{2+}-doped materials are of interest because of their suitability for broadband optical amplifiers and for optical communications. The effect of Ni^{2+} ions on structure and dielectric properties of materials was also studied [16-19]. For targeting broadband light amplification, transparent glass- ceramics are rather suitable because they can be used to fabricate fiber devices. Ni^{2+}-doped transparent glass-ceramics are typically obtained by specially designed secondary heat-treatments of initial glasses with proper compositions. This ensures precipitation of desired nanocrystalline phases offering octahedral site symmetry for Ni^{2+} ions and maintains the material transparency.

Recently developed Ni-dope spinel nanostructures [10,11] demonstrated optical and magnetic bifunctional properties that have promising potential application in the fields of magnetic information storage, biological diagnosis and optical communication. Transparent NiO-doped glass-ceramics containing various crystals with spinel structure were successfully elaborated as well. They demonstrate broadband emission in the near-IR [20-37]. In these glass-ceramics, emitting centers are Ni^{2+} ions located in spinel nanocrystals in octahedral coordination sites. The stoichiometry of spinel can vary significantly [38-41], Mg-Al spinels are represented as $MgO\text{-}nAl_2O_3$, for n=1 it is stoichiometric and any other value of n results in non-stoichiometric spinels. The structure of spinels with the general formula AB_2O_4, where A ions are located in tetrahedral sites and B ions in octahedral sites (normal

spinel), is rendered complicated by disordering of the cations between the A and B sites (intermediate and inverse spinels) [42,43]. $MgAl_2O_4$ is a normal spinel, with space group *Fd*3*m*. There are 8 formula units per cell with the oxygen ions forming a cubic close-packed struc- ture. The Al^{3+} and Mg^{2+} ions have octahedral and tetrahedral co- ordination with oxygen, respectively.

$MgAl_2O_4$ spinel demonstrates the effect of rapid disordering of Mg and Al cations at high temperatures and subsequent quenching of disorder when the spinel is rapidly cooled down to ambient temperature. The distribution of Ni^{2+} ions between octahedral and tetrahedral sites depends upon spinel composition, NiO concentration and conditions of preparation (temperature, time, pressure, *etc*.) [44]. The detailed knowledge of regularities of phase separation and crystallization of Ni^{2+}-doped glasses, distribution of Ni^{2+}ions between different phases in glass-ceramics and between octahedral and tetrahedral sites in spinel crystals allows for con- trolling the luminescence efficiency of the material in the near-IR [33,45]. In spite of the fact that spinel-based glass-ceramics of the $MgO\text{-}Al_2O_3\text{-}SiO_2$ system were developed long ago, we found only one paper on luminescent properties of Ni^{2+}-doped spinel-based glass-ceramics of the $MgO\text{-}Al_2O_3\text{-}SiO_2\text{-}TiO_2$ system [25]. Wu et al. demonstrated this glass-ceramic is a promising material for applications in tunable lasers and broadband amplifiers. However, due to incorrect attribution of the magnesium aluminotitanate phase to b-quartz solid solution [25], the authors concluded that spinel was the secondary phase precipitated additionally to b-quartz solid solution [27], and moved their research activity to gallium-doped spinel-based MAS glass-ceramics [27]. We did not find any study of luminescent properties of Ni^{2+}-doped spinel-based glass-ceramics of the $MgO\text{-}Al_2O_3\text{-}SiO_2$ system nucleated by TiO_2 and ZrO_2.

In Ref. [46], the Ni environment in the glass and the glass-ceramics of the MAS ternary system with ZrO_2 and TiO_2 was sys- tematically investigated *in situ* at high temperature using optical absorption spectroscopy and X-ray absorption spectroscopy. The aim of the present study is to follow the structural evolution of MAS glass-ceramics of the optimized composition nucleated by a mixture of ZrO_2 and

TiO_2 and doped with NiO prepared at different heat-treatment temperatures and to connect it with the evolution of luminescence characteristics of glass-ceramics. The detailed analysis of the luminescent properties of glass-ceramics in relation to structure of the emitting centers is essential for the development of new luminescent materials. We expected that randomization of the spinel structure in glass-ceramics prepared by high- temperature heat-treatments and its ordering in subsequent low-temperature heat-treatments will be revealed in the intensity of the luminescence signal. To the best of our knowledge, it is the firsttime that such study is performed.

2. Experimental

2.1. Sample preparation

Magnesium aluminosilicate glasses with the composition (mol %) 20 MgO, 20 Al_2O_3, 60 SiO_2 were prepared with the addition of nucleating agents (TiO_2 and ZrO_2) and NiO. The nominal glass compositions are 18.0 MgO, 18.0 Al_2O_3, 54.0 SiO_2, 4.5 TiO_2, 4.5 ZrO_2, 1.0 NiO and 17.95 MgO, 17.95 Al_2O_3, 53.9 SiO_2, 4.5 TiO_2, 4.5 ZrO_2, 1.2 NiO (mol%). Glasses were melted at 1580°C for 4 h (h) under stir- ring, poured onto a cold metal plate and annealed at 660°C. Then one-stage heat-treatments at 800°C for 3 and 6 h were applied. In two-stage heat-treatments, the first heat-treatment at 800°C for 3 h was accompanied by the second one either at 850°C or at 950°C for 3 h. In another heat-treatment schedule, the temperature and the duration were selected as follows: 1) 800°C for 1-3 h, 2) 850°C for 1-3 h, 3) 950°C for 1-3 h and 4) 850°C for 193 h. Based on preliminary studies [33], the duration and the temperature of these heat-treatments were optimized in order to investigate structural changes in a reasonable experimental time.

2.2. X-ray diffraction

X-ray diffraction (XRD) analysis was carried out on a PANalytical X'Pert PRO diffractometer with nickel-filtered Cu Kα radiation. XRD patterns were acquired *in situ* at high temperature using an Anton Paar HTK 1200 furnace, over an angular range 24°≤2θ≤60° with an acquisition time of 30 min. We have selected this angular range to reduce the acquisition time. The main diffraction peaks of the studied crystalline phases are clearly visible on such XRD patterns. Coarse powders were used to limit surface crystallization. Crystalline phases were determined using the X-Pert High Score Plus software [47].

XRD patterns of powdered samples were also measured with a Shimadzu XRD-6000 diffractometer with nickel-filtered Cu Kα radiation over an angular range 24°≤2θ≤80°. The mean crystal sizes were estimated from broadening of X-ray peaks according to Scherrer's equation:

$$D = K\lambda/\Delta(2\theta)\cos\theta, \qquad (1)$$

where K is a constant assumed to be 1 [48], λ is the wavelength of X- ray radiation, θ is the diffraction angle, and $\Delta(2\theta)$ is the full width at half maximum. The error in the mean crystal size estimation is about 5%. The unit cell parameter a was estimated from the position of the (440) plane of the spinel crystal. Relative amounts of spinel were estimated by measuring intensity of the diffraction peak of spinel around 2θ=45°, which corresponds to the reflection from the (400) plane.

2.3. *Raman spectroscopy*

Unpolarized Raman spectra were measured in backscattering geometry on an InVia (Renishaw, England) Micro-Raman spectrometer equipped with the multichannel detector cooled up to 70°C. The spectra were excited by Ar^+ CW laser line of 514 nm. Leica 50 (N.A. 0.75) objective was used for illuminating the sample; the scattered light was collected by the same objective. Edge filter was placed before the spectrograph entrance slit; a spatial resolution was of 2 cm^{-1} and acquisition time was 50 s.

2.4. *Optical spectroscopy*

The UV-visible-NIR absorption spectra of polished samples in the UV, visible and near-IR were carried out *in situ* in the temperature range from 25 to 950°C in transmission mode on a Perkin Elmer Lambda 1050 spectrometer in the range between 400 and 1700 nm (from 6000 to 25000 cm^{-1}) with a 2 nm step. Absorbance spectra were normalized to the sample thickness and Ni^{2+} concentration. The samples with diameter of 1-3 cm and thickness of 0.5-1 mm were held between two sapphire windows, placed inside a heating stage (Linkam TS1500) using a special set-up [49]. The heating rate between the temperature plateaus was set to 100°C / min. The speed of data acquisition (10 min) allows the determination of kinetics information on the local structural changes around Ni^{2+} ions during phase transformations in the glass matrix.

Room-temperature absorption spectra were recorded also by using a double-beam spectrophotometer (Shimadzu UV 3600) in the range between 2500 and 250 nm (from 4000 to 40000 cm^{-1}). The samples were 1 mm-thick polished plates. Absorbance spectrawere normalized to the sample thickness.

2.5. *Photoluminescence properties*

For investigation of photoluminescence (PL) spectra and decay curves, the glass samples doped with 1 mol% NiO (1 mm-thick polished plates) were heat-treated according to the heat-treatment schedules listed above, namely at 800°C for 3 h, and then sequentially at 850°C for 1-3 h, at 950°C for 1-3 h and again at 850°C for 1-3 h (in increments of 1 h).

PL was excited at 960 nm by focused radiation of CW 1 W InGaAs laser diode. It was collected in orthogonal direction by a wide-aperture lens, reimaged to the input slit of a monochromator (SBW 2 nm) and then detected with a lock-in amplifier and a Hamamatsu G5851 photodetector. The spectrum was measured in the spectral range

of 1000-1800 nm.

For time-resolved study, laser output from an optical parametric oscillator (20 ns pulse duration) was used. The detection system was similar to that described above for the PL experiment (a 500 MHz digital oscilloscope was also used). Excitation was per- formed closely to additionally polished side face of the sample in order to avoid reabsorption and scattering losses.

3. Results

The regularities of phase transformations were studied using the glass doped with 1.2 mol% NiO. Initial glass with a brown coloration is transparent (Fig. 1). After heat-treatment at the nucleation stage, 800℃ for 3 h, there is no color change. After heat treatment at the second stage at 850°C for 3 h, it becomes green; after the third hold at 950°C for 3 h, the color changes to blue turquoise, after the next hold at lower temperature, it becomes slightly darker. The materials remain transparent after these heat- treatments.

3.1. X-ray diffraction study

In situ XRD measurements are useful to study the kinetics of crystal phase precipitation and to determine the crystallization sequence in details. The initial glass shows no Bragg peaks using X-ray diffraction (Fig. 2a). Similar to Ref. [42], a Bragg peak at 2θ of about 30° appears just after the heat-treatment for 0.5 h at 800°C. Owing to very small particle sizes and small quantity of crystals, it is difficult to attribute this phase unambiguously to $ZrTiO_4$ [46,50,51] or to disordered $(Zr,Ti)O_2$ solid solution [52,53]. The peak at 2 θ~30° slightly increases in intensity during this temperature stage and becomes narrower owing to the increase of the crystal size.

After the heat-treatment at 850°C only for 0.5 h, additional peaks at 37° and 45° can be detected due to spinel crystallization. The anomalously high intensity of the

peak at 30-3° justifies a superposition of the spinel peak with the main peak of the zirco- nium titanate phase. The intensity of all peaks increases with time and with increasing temperature up to 950°C. The peaks at 50° and 59° (the latter is clearly seen in spite of the fact that the XRD pat- terns were recorded till 60°) are also observed indicating higher volume concentrations of the zirconium titanate and spinel crystals, respectively. Additional holding at 850°C for 0.5-3 h does not show any change in the phase composition of the glass-ceramic sample (not shown).

With the aim to confirm *in situ* XRD findings, we made similar heat-treatments in an annealing furnace and performed an XRD analysis of the samples (Fig. 2b). It provided a better signal-to-noise ratio for the XRD patterns. According to XRD analysis (Fig. 2b), after heat-treatment at 800°C for 3 h, crystals of $ZrTiO_4$ are detected. Their fraction increases when the duration of heat-treatment increases to 6 h, while spinel crystallizes additionally at elevated temperatures of 850°C and 950°C. These data correspond to the *in situ* XRD data.

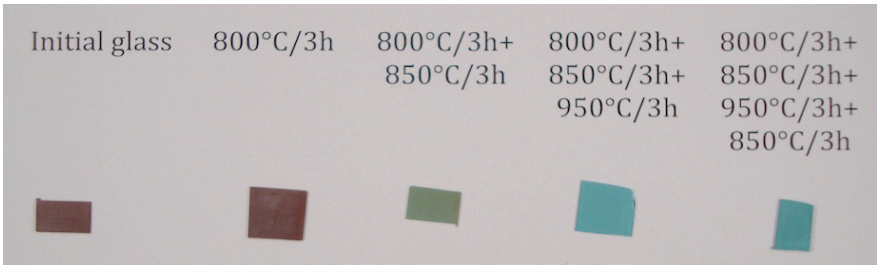

Fig. 1. Color variation in glass and glass-ceramics doped with 1.2 mol% NiO after different stages of heat treatment.

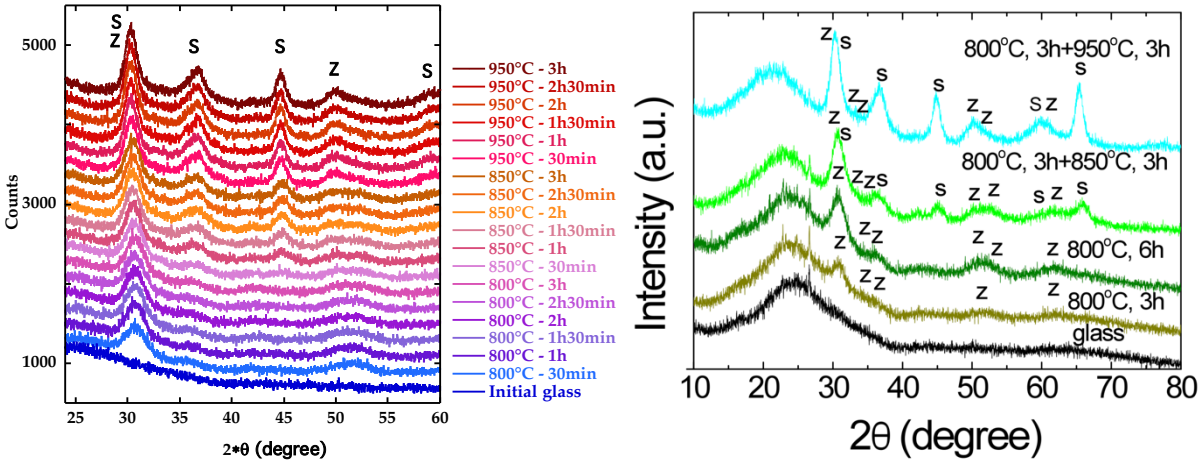

Fig. 2. (a) High temperature XRD patterns of the glass sample doped with 1.2 mol% NiO measured successively at 800°C, 850°C and 950°C as a function of time. (b) *Ex situ* XRD patterns of the initial and heat-treated glass doped with 1.2 mol% NiO. The numbers indicate the heat-treatment schedules. The "S" and "Z" labels indicate the XRD peaks attributed to spinel and $ZrTiO_4$, respectively. The patterns are shifted for the convenience of observation.

3.2. ***Raman spectroscopy study***

The Raman spectrum of the initial glass doped with 1.2 mol% NiO (Fig. 3) demonstrates the middle-range band with a maximum at ~460 cm^{-1} and a broad high-frequency envelope with two pronounced maxima at ~800 cm^{-1} and 920 cm^{-1} and a smaller peak at ~1100 cm^{-1}. The Raman spectrum of the same magnesium aluminosilicate glass without nucleating agents [54] has broad bands being characteristic for aluminosilicate network, appearing at ~470 cm^{-1} and associated with motions of bridged oxygen in T-O-T linkages, where T is Si or Al [55], at ~800 cm^{-1} (assigned to Si-O stretching of different origin [56]), and at ~1015 cm^{-1} (assigned to stretching vibrations of the fully polymerized tetrahedral Si(OAl)*y* network units, where *y* is the number of AlO_4 tetrahedra connected to a SiO_4 tetrahedron [55] or to (Si,Al)-NBO and (Si,Al)-BO (NBO denotes non-bridging O atoms and BO bridging O

atoms) stretch bands [57]). The Raman spectrum of the initial magnesium aluminosilicate glass of the same base composition nucleated solely by ZrO_2 [58] is very similar to the spectrum of the base glass without any nucleating agent. It does not have any high frequency band at about 900 cm^{-1}.

The Raman spectrum of amorphous ZrO_2 contains three distinct peaks at 148, 263 and 476 cm^{-1} assigned to small ordered regions that do not produce diffraction peaks, and a very wide envelope in the middle-frequency region with a tail which spans to 750- 800 cm^{-1} [59] while the Raman spectrum of amorphous $ZrTiO_4$ has broad bands at 145, 290, 410, 645 and 780 cm^{-1} [60]. Thus, in the Raman spectrum of the initial glass under study, the broad band at about 920 cm^{-1} should be related to the presence of titania. Indeed, the [TiO_4] tetrahedra are known to enter the silicate network, which leads to the appearance of a rather intense Raman band at ~ 910 cm^{-1} [54,61-64]. In the Raman spectrum of the glass under study with a mixture of nucleating agents, the high-frequency band is located at about 920 cm^{-1}, in contrast to its position of ~900 cm^{-1} in the Raman spectrum of the same glass doped only by TiO_2 [54].

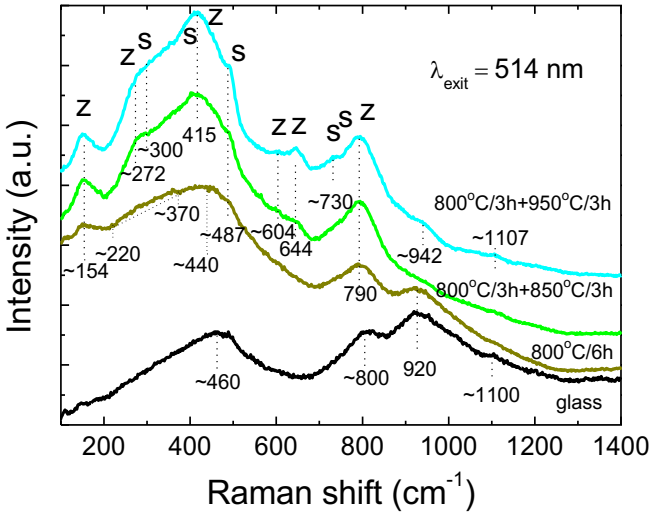

Fig. 3. Raman spectra of initial and heat-treated glasses doped with 1.2 mol% NiO. The “S” and “Z” labels indicate the Raman peaks attributed to spinel and $ZrTiO_4$, respec- tively. The excitation wavelength is 514 nm. The spectra are shifted for the convenience of observation.

We can assume that this difference is caused by the presence of zirconium ions in the glass network. Possible incorporation of zirconium ions in the silicate network could lead to a change of lengths and of elastic constants of the bonds between the [TiO_4] and [SiO_4] tetrahedrons (Ti-O-Si), which could result in the shift of a Raman band of 20 cm^{-1}. This effect of Zr on the position of this band could be an indirect indication of the close proximity of Ti and Zr ions.

After the heat-treatment at 800°C for 6 h, the Raman spectrum changes pronouncedly: the main middle-range band is shifted to ~440 cm^{-1}, and a redistribution of intensity in the spectrum of the high-frequency band in favor of the band at ~790 cm^{-1} (Fig. 3) is observed. A very weak broad band at 220-370 cm^{-1} is superimposed on the low-frequency side of the band at about 440 cm^{-1}. A similar very broad and weak band at ~220-370 cm^{-1} was observed earlier in Raman spectra of glasses of the zinc alumino-silicate system nucleated by a mixture of TiO_2 and ZrO_2 and containing nickel oxide [45]. There is also a band at 154 cm^{-1}. The changes in the Raman spectrum of the sample heat-treated at 800°C testify the phase separation of glass and appearance of Ti,Zr- containing phase. The peak at 154 cm^{-1} is probably due to formation of inhomogeneous regions enriched with zirconium and titanium oxides and crystallization within these regions [60,65-68], which is confirmed by XRD data (crystallization of the zirconium titanate crystals). A decrease in intensity of the band at ~920 cm^{-1} and a simultaneous growth of the band at ~790 cm^{-1} (as well as in the spectrum of the MAS glass nucleated solely by TiO_2 [54]) is associated with the titanium coordination change. The main contribution to the intensity of the band ~790 cm^{-1} is connected with titania polyhedra with coordination higher than 4 and with possible distortions as a result of liquid phase separation with formation of amorphous aluminotitanate phase, which, apparently, includes zirconium, magnesium and nickel ions. The shift of the position of the main Raman band from 460 cm^{-1} (motions of bridged oxygen in T-O-T linkages, where T is Si or Al [55]) to ~ 440 cm^{-1} (the position characteristic for the Raman spectrum of vitreous silica [69]), is also a result of phase separation of the initial glass because the silicate matrix becomes depleted by titanium and zirconium oxides.

The spectral changes are increased after two-stage heat-treatments with a

second stage at 850 and 950°C. After the two-stage heat-treatment at 800°C for 3 h and at 850°C for 3 h, intensity of the broad band at ~790 cm^{-1} increases at the expense of the band located at 920 cm^{-1} and the bands at 154, ~276, 415, ~487 and 646 cm^{-1} arise. After heat-treatment at 800°C for 3 h and at 950°C for 3 h, two additional bands evolve at ~600 and ~728 cm^{-1}. For zirconium titanate crystals, the characteristic bands are located at 154-158, 269, 331, 415, 590, 646 and 795 cm^{-1}, of which the most intense are bands at 154e158, 269, 415 and 646 cm^{-1} [65-68]. Therefore, most of the Raman bands observed in the studied spectra can be attributed to zirconium titanate (Table 1). Among all the Raman bands characteristic for $MgAlO_4$ spinel [70-72], only that at ~730 cm^{-1} is clearly seen in the Raman spectrum, and it is only in the spectrum of glass-ceramics prepared at the highest temperature (by the two-stage heat-treatments with the second hold at 950°C). All other spinel bands, including the most intense Raman band located at ~410 cm^{-1}, are not apparent, which is probably because they are overlapped by more intense and broad bands due to zirconium titanate and the residual glass (see Table 1). We doubt the band at ~487 cm^{-1} can be attributed to spinel, because in this case, according to Ref. [71], its intensity would have been several times weaker than that of the peak at ~410 cm^{-1}. H. Cynn et al. [71] demonstrated that the band at ~730 cm^{-1} can be assigned to a fundamental Raman-active vibration of AlO_4 tetrahedra, created by redistribution of some aluminum ions from octahedral to tetrahedral sites. Thus, the Raman spectrum bears the evidence of spinel disordering with the increase of heat-treatment temperature from 850 to 950°C. The broad bands of low intensity at ~942 and ~1107 cm^{-1} that appear in the Raman spectrum of the glass-ceramics prepared by the second hold at 950°C suggest that a small amount of titanium ions remains in the residual highly siliceous glass [73].

Table 1. Experimental Raman frequencies (in cm^{-1}) for $ZrTiO_4$ according to [51-54], for synthetic $MgAl_2O_4$ [56-58] and present glass-ceramics.

$ZrTiO_4$	$MgAl_2O_4$	Glass-ceramics, 800 °C, 6 h	Glass-ceramics, 800 °C, 3 h + 850 °C, 3 h	Glass-ceramics, 800 °C, 3 h + 950 °C, 3 h
154-160		154	151	149
269-290		~280	~276	~276
	~310		~300	~300
320-331				
400-415	~410		415	415
		440		
	490 [57]	~487	~487	~487
566-590				
603-626			604	604
637-646	670		644	644
	727		730	730
	770			
792-802		790	790	790

3.3. Optical absorption spectroscopy

The optical absorption spectrum of the initial glass (Fig. 4) is very similar to the previously obtained one for the same Ni-bearing magnesium aluminosilicate base glass nucleated by a larger content of nucleating agents, 6 mol% TiO_2 and 6 mol% ZrO_2 [46]. It is interpreted as mainly fivefold coordinated Ni^{2+} in trigonal bipyramid ($^{[5]}Ni$) sites (22 900 cm^{-1} band) with a small amount of tetrahedral ($^{[4]}Ni^{2+}$) sites (15 500 cm^{-1} band) [46]. A detailed interpretation of absorption bands can be found elsewhere [33,74].

In the absorption spectrum of the glass heat-treated at 800°C for 3 h and for 6 h, a pronounced red shift of the absorption edge is clearly visible. The main part of the spectrum remains unchanged after 3 h of heat-treatment while the intensity of the characteristic band of five-fold coordinated Ni^{2+} ions slightly decreases after the 6 h holding. The shift of the absorption edge indicates liquid phase separation and beginning of $ZrTiO_4$ crystallization (Fig. 2). Indeed, $ZrTiO_4$ has an optical band gap at 3.09 eV [68], and its crystallization causes the shift of the absorption band edge [75].

At 850°C, in- tensities of all $^{[5]}Ni^{2+}$ and $^{[4]}Ni^{2+}$ bands in glass decrease because of formation of the $^{[6]}Ni^{2+}$ and $^{[4]}Ni^{2+}$ species in spinel nanocrystals. Absorption bands due to $^{[6]}Ni^{2}$ species that are above 25 000 cm^{-1} overlap with the UV-absorption edge. $^{[6]}Ni^{2+}$ species also contribute to bands at about 16 000 cm^{-1} and 9000 cm^{-1} [5,7]. A broad band at 16 600 cm^{-1} can be connected with absorption of $^{[4]}Ni^{2+}$ and $^{[6]}Ni^{2+}$ sites that appear during spinel crystallization superimposed with absorption of $^{[4]}Ni^{2+}$ sites still remaining in the residual glass. The color of the sample changes to green (Fig. 1).

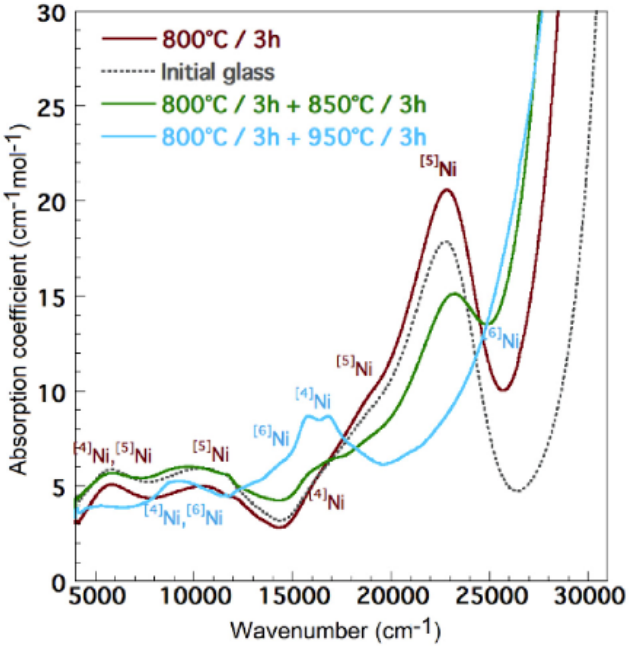

Fig. 4. Optical absorption spectra of the initial and heat-treated glasses doped with 1.2 mol% NiO.

When increasing the heat-treatment temperature to 950°C, we observe a pronounced decrease of the intensity of the $^{[5]}Ni^{2+}$ and $^{[4]}Ni^{2+}$ bands in the residual glass. It is especially clear from the absence of the $^{[5]}Ni^{2+}$ band at ~22 900 cm^{-1}. Ni^{2+} ions are strongly partitioned between the $^{[4]}Ni^{2+}$ and $^{[6]}Ni^{2+}$ sites in spinel. This

coordination change causes the change in coloration of the sample from green to blue turquoise (Fig. 1).

3.4. *In situ UV-Visble-NIR spectra*

In situ UV-Visible-NIR absorption spectroscopy (Fig. 5) not only confirmed the variations of absorption spectra with heat- treatments (Fig. 4), but also gave additional information on kinetics of spectral transformations. From the absorption spectra measured during the isotherm at the 800 °C hold, one can see that the spectral changes begin as soon as $ZrTiO_4$ crystals start precipitating, and the band intensity of the $^{[5]}Ni^{2+}$ ions at above 20000 cm^{-1} decreases at this stage, which suggests the beginning of the $^{[6]}Ni^{2+}$ ions formation. Indeed, Ni^{2+} ions can enter into the structure of $ZrTiO_4$ crystals, where they are located in distorted octahedral sites [76]. The spectra are changed pronouncedly as soon as the temperature is raised to 850°C, so that the beginning of the spinel precipitation is accompanied by the rapid decrease of the $^{[5]}Ni^{2+}$ fraction and increasing of the $^{[6]}Ni^{2+}$ fraction. Almost no change is observed in the absorption spectrum after 2 h of heat- treatment at 850°C. Absorption bands in the visible and in the NIR spectral regions associated with Ni^{2+} absorption in spinel nanocrystals become more distinct after additional heat-treatment at 950°C for 20 min. Further holds let the spectrum near unchanged. No spectral change was found after the additional heat- treatment at the lower temperature of 850°C (not shown here).

The second part of the research, the search for the correlation between the structure, absorption and luminescence properties of Ni-doped spinel-based glass-ceramics was performed using the samples of the same composition doped with 1 mol% NiO. They were heat-treated successively at 800°C, 850°C, 950°C and again at 850°C. All the measurements were performed at room temperature. The features of phase transformations revealed for glasses doped with 1 and 1.2 mol% NiO were rather similar.

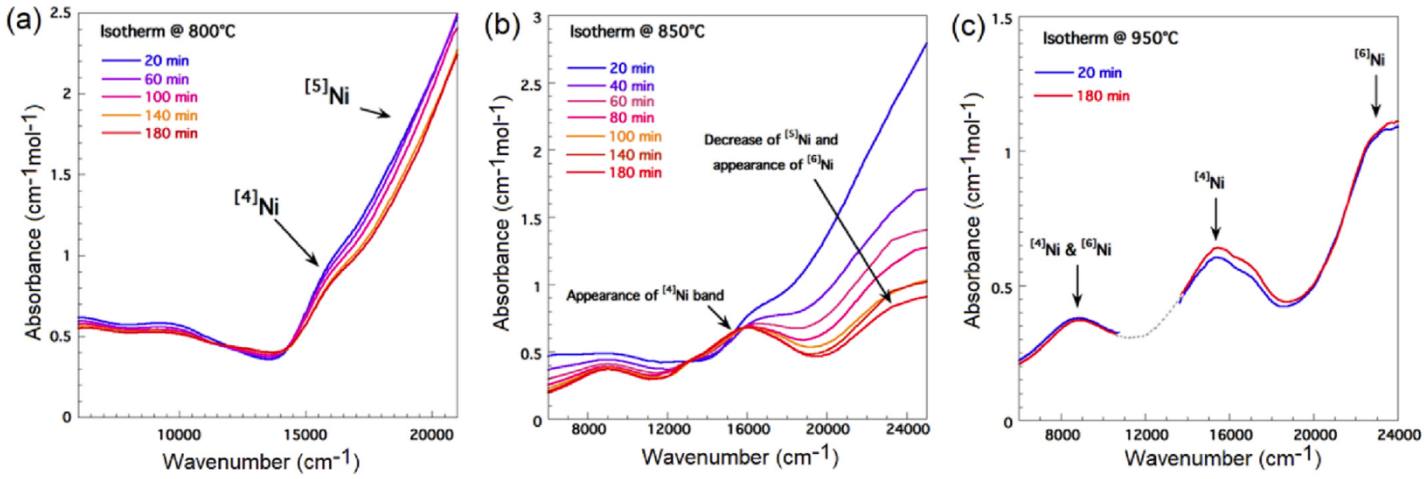

Fig. 5. Isothermal measurements carried out on the heat-treated glasses doped with 1.2% NiO and measured successively at (a) 800°C, (b) 850°C and (c) 950°C as a function of time. The grey dotted line on the isotherm at 950°C is a guide for the eyes.

3.5. *Luminescence study*

The initial glass and samples heat-treated at 800°C for 1-3h show no near-IR PL. In contrast, the sample heat-treated at the first stage at 800°C for 3 h and at the second stage at 850°C for 1 h and those with subsequent heat-treatments are characterized by an intense and broad PL band spanning across the range of 1.0e1.8 mm and related to the $^3T_2$ (^3F)→$^3A_2$ (^3F) radiative transition for Ni^{2+} ions located in octahedral sites in spinel nanocrystals [6,7]. The PL spectra are summarized in Fig. 6. Their analysis (the values of integrated PL intensity, peak wavelength l_{peak}, full width at half maximum, FWHM, and the mean PL decay time), is presented in Fig. 7a-c. With the increase of the heat-treatment duration, the PL properties of glass-ceramic samples are changed. The PL intensity is increased continuously (the most noticeable change occurs during heat-treatments at 850 and 950°C), l_{peak} is shifted to shorter wavelengths (from 1325 to 1300 nm), and PL band becomes more narrow, with the decrease of the FWHM from 380 to 310 nm.

The measured PL decay curves were clearly not single- exponential (see below). Thus, we applied the stretched exponential function [77] for their fitting:

$$I(t)=I_0\exp(-(t/\tau)^{ß}) \qquad (2a)$$

$$<\tau>=(\tau/ß).\Gamma(1ß) \qquad (2b)$$

Here, τ is the decay time, $0 < \mathbf{b} < 1$ is the dispersion factor (ß=1 for a single-exponential decay), $<\tau>$ is the mean decay time and Γ is the gamma-function.

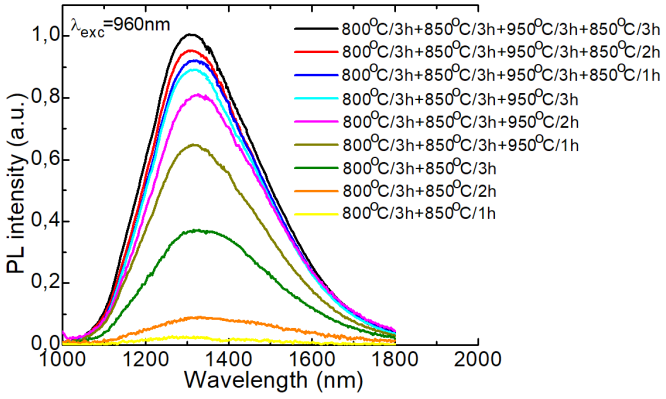

Fig. 6. Emission of Ni^{2+} ions in octahedral sites (the $^3T_2(^3F)\rightarrow{}^3A_2(^3F)$ transition) for studied glass-ceramics doped with 1 mol% NiO for various heat-treatment schedules.

4. Discussion

The increase of the PL intensity at increasing and further decreasing the heat-treatment temperature (Figs. 6 and 7) requires discussion. For explanation of the results of PL study, the detailed XRD analysis of the same samples containing 1.0 mol% NiO that were used for the luminescence measurements was performed. The crystal sizes of both phases (spinel and $ZrTiO_4$), the spinel lattice parameters and the relative intensity of the spinel peak (400) were estimated (Fig. 8a and b and Table 2). The sizes of spinel and $ZrTiO_4$ crystals increase with temperature and duration of heat-treatments at 850°C and 950°C and remain near constant after additional heat-treatment at 850°C. Increasing the heat-treatment temperature leads to an abrupt

increase in the crystal size while the rate of the crystal size growth at every stage decreases with the heat- treatment duration.

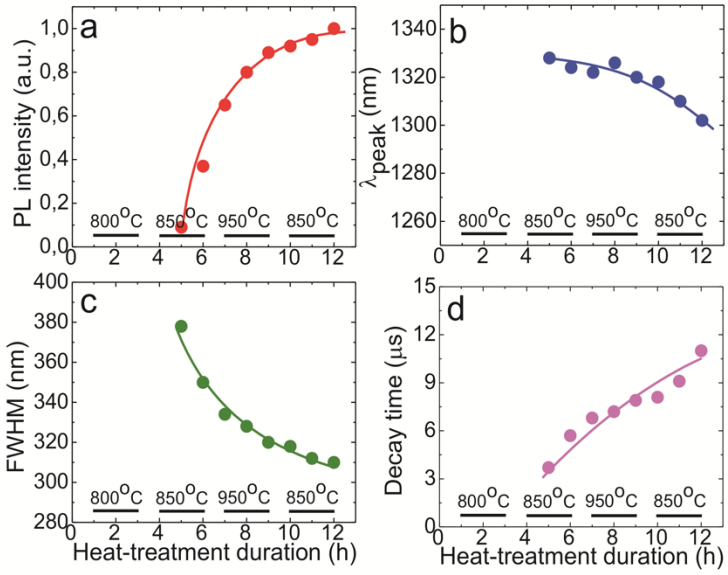

Fig. 7. Integrated PL intensity (a), peak wavelength (b), FWHM of emission band (c) and mean PL decay time (d) for the studied glass-ceramics doped with 1 mol% NiO for various heat-treatment schedules.

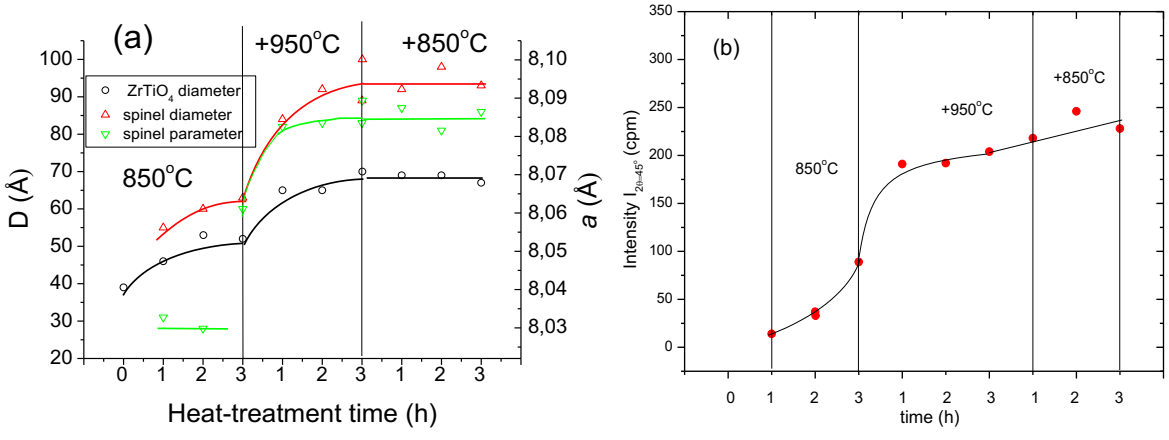

Fig. 8. (a) Dependence of crystal size and spinel lattice parameter on the heat- treatment schedule. (b) Dependence of intensity of the spinel peak (400) on the heat-treatment schedule. The error matches the size of symbols.

The lattice parameter *a* increases from 8.030 ± 0.003 Å for spinel crystallized at 850 °C for 1-2 h to 8.085 ± 0.003 Å for that crystallized at 950°C. It does not change significantly after additional heat-treatment at 850°C. These values of the lattice constant imply that the composition of the spinel under study is enriched in alumina and the increase of the lattice constant with heat- treatment temperature could be explained by the decrease of the excess of aluminum in the spinel composition [78].

The spinel growth rate rapidly increases with heat-treatment time at 850°C and with raising the temperature to 950°C. An in- crease in the heat-treatment time at 950°C leads to cessation of the spinel crystals growth after ~3 h. Additional heat-treatment at 850°C results in some increase of the amount of spinel crystals precipitated.

Table 2. Characteristics of crystalline phases precipitated in glass-ceramics under study.

Heat-treatment schedule, °C / h	$ZrTiO_4$	Spinel		
	D, Å	*D*, Å	*a*, Å	Intensity $I_{(400)}$
800/3	39	-	-	-
800/3+850/1	46	55	8.031	14
800/3+850/2, taken from the furnace	53	64	8.029	33
800/3+850/3	52	63	8.060	89
800/3+850/3+950/1	65	82	8.082	191
800/3+850/3+950/2	65	92	8.083	192
800/3+850/3+950/3	70	89	8.083	204
800/3+850/3+950/3+850/1	69	92	8.087	218
800/3+850/3+950/3+850/2	69	98	8.081	246
800/3+850/3+950/3+850/3	67	93	8.086	228

The impressive variation of the absorption spectra at the heat- treatment of 850°C for 1-3 h (the pronounced decrease of the $^{[5]}Ni^{2+}$ fraction in the initial glass and increase of the $^{[6]}Ni^{2+}$ fraction) corresponds to the fast spinel formation, Fig. 8b, and it is accompanied by the increase of the PL intensity (Fig. 6). The additional spinel crystallization at 950°C for 1 h leads to increasing the Ni^{2+} absorption bands associated with Ni^{2+} in spinel crystals. The continuation of the heat-treatment at this temperature results in the change in the absorption spectrum shape, probably

due to increasing amount of Ni^{2+} in octahedral sites at the expense of tetrahedral ones, Fig. 9b. The PL intensity concomitantly increases (Fig. 6). After the low-temperature heat-treatment at 850°C, which results in some increase in fraction of spinel crystals (Fig. 8b), the shape of the spectrum remains near unchanged (Fig. 9c) but the PLintensity still increases.

The similar evolution of the PL properties as found in the pre- sent study was observed in Ref. [33] for gahnite-containing glass- ceramics. Partially such variations can be attributed to redistribution of Ni^{2+} ions over both octahedral and tetrahedral sites. In this way, blue-shift of I_{peak} and narrowing of the PL band arise from ordering of spinel structure and increase in the ligand field strength, so that PL spectrum becomes more similar to that of the spinel single crystal [8]. It can be related largely with an increase of volume fraction of Ni^{2+}-containing spinel nanophase and growth of individual nanocrystals. The latter is supposed to be related to a process of non-radiative relaxation for Ni^{2+} ions located near the nanocrystal surface that can suppress PLintensity. The impact of this process can be easily recognized with time-resolved studies that were performed in present paper.

PL decay curves for glass-ceramics heat-treated at (800°C for 3 h and 850°C for 2 h) and at (800°C for 3 h, 850°C for 3 h, 950°C for 3 h and 850°C for 3 h) are shown in Fig. 10. The decay curves plotted in a semi-log scale are clearly non-linear, which can be related to the existence of distorted octahedral sites for Ni^{2+} ions (indeed, spinel structure is disturbed in the interface of the residual glass and nanocrystals). Typical values of mean decay time τ, Eq. (2), are several μs that is substantially shorter than 108 μs listed in Ref. [25]. However, as it was shown in Ref. [30], such shortening results from a strong impact of concentration quenching effect for samples with NiO content higher than 0.1 mol%. The value of τ is increased by a factor of four, namely from 3.54 to 14.74 μs, with the change of heat-treatment schedule, Fig. 10. This supports our idea about the reduced influence of the non-radiative path due to the growth of fraction of Ni^{2+} ions located in the volume of spinel nanocrystals as compared to those located near the nanocrystal surface. The effect of spatial

distribution of luminescent centers on non-radiative path was studied previously in Ref. [79].

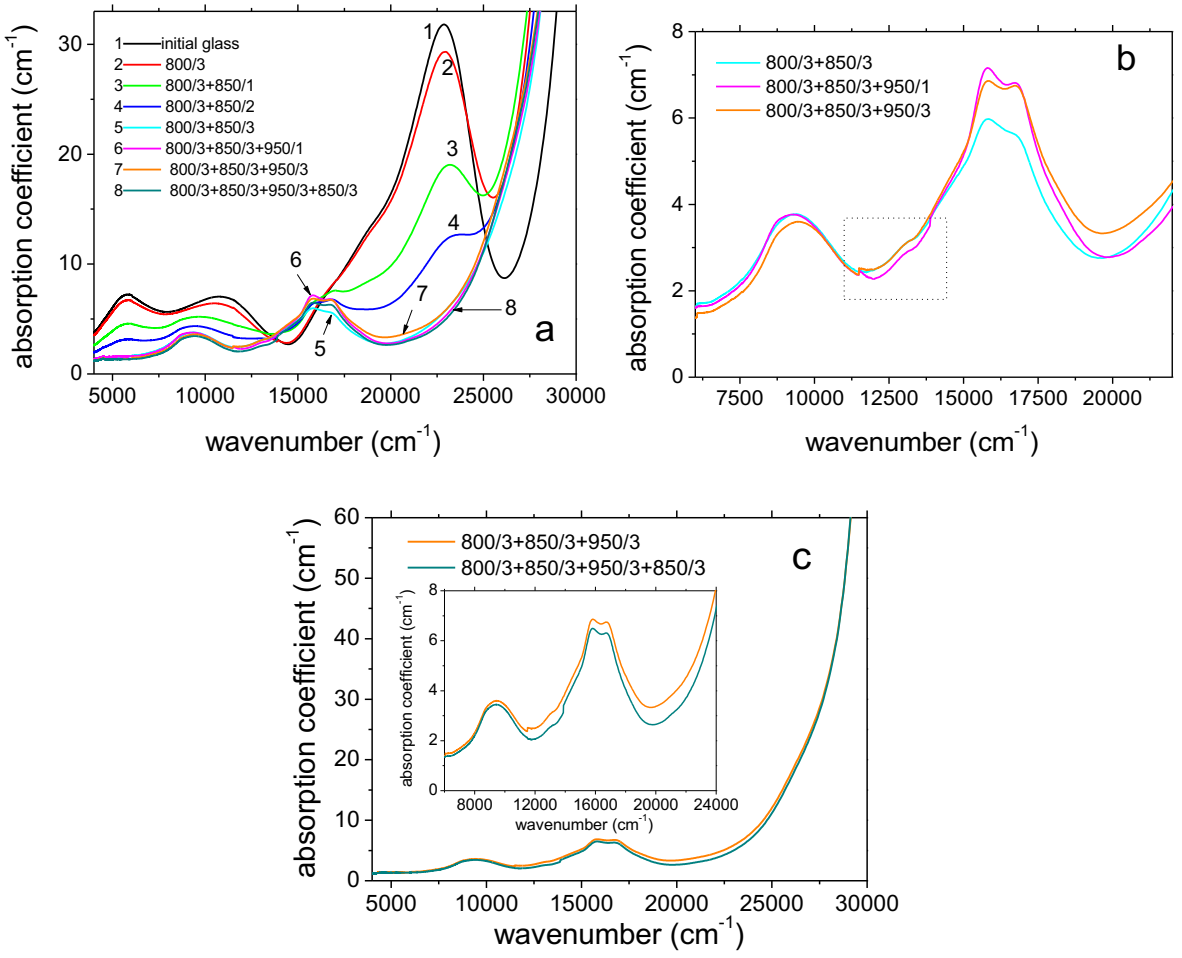

Fig. 9. (a-c) Room-temperature absorption spectra of the glasses doped with 1 mol% NiO and subjected to different single-stage and multi-stage heat-treatments. The *dashed region* corresponds to switching the detectors. The *numbers* indicate temperature/duration of the heat-treatment, in °C/hours, respectively.

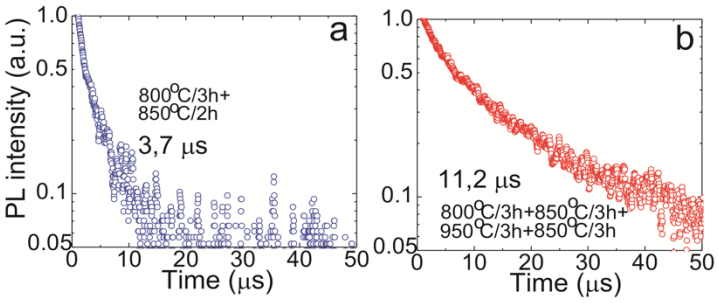

Fig. 10. PL decay curves for samples of studied glass-ceramics (1.0 mol% NiO) with different heat-treatment schedules: *symbols* - experimental data, *curves* - their fitting with the stretched exponent model, Eq. (2), τ is the mean decay time. The excitation wavelength is 960 nm, the luminescence is detected at 1300 nm. The numbers indicate temperature/duration of the heat-treatment, in °C /hours, respectively.

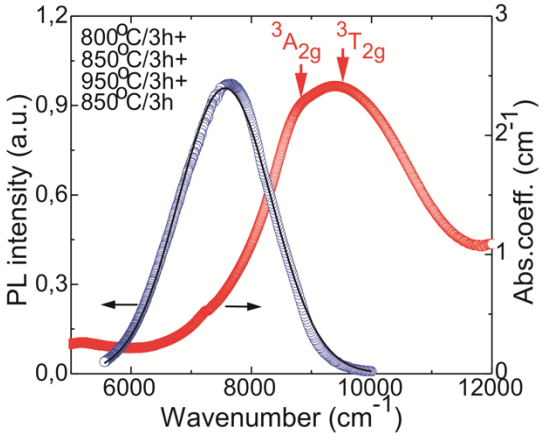

Fig. 11. Near-infrared absorption and emission spectra of Ni^{2+} ions for the glass-ceramics obtained by the heat-treatment at 800°C for 3 h + 850°C for 3 h + 950°C for 3 h + 850°C for 3 h (1.0 mol% NiO). *Symbols*: experimental data, *solid curve*: Gaussian fitting of the PL band, *arrows* denote absorption and emission bands related to Ni^{2+} ions positioned in the octahedral ($[6]Ni^{2+}$) and tetrahedral ($[4]Ni^{2+}$) sites.

Fig. 11 shows analysis of relative position of absorption and PL bands for glass-

ceramic sample heat-treated at 800°C for 3 h, 850°C for 3 h, 950°C for 3 h and 850°C for 3 h. Here, symbols correspond to the measured spectra, solid line - to Gaussian fitting of the PL band. The difference of FWHM of these bands (2940 cm^{-1} for absorption and 1820 cm^{-1} for PL), the difference in their shape and good applicability of Gaussian fitting to the PL one (considering the impact of reabsorption at short wavelengths) are the indications of the presence of two types of sites for Ni^{2+} ions in the spinel structure. Indeed, these are octahedral ($^{[6]}Ni^{2+}$) and tetrahedral ($^{[4]}Ni^{2+}$) ones. The corresponding transitions $^3A_2(^3F)$ / $^3T_2(^3F)$ for $^{[6]}Ni^{2+}$ and the $^3T_2(^3F)$ / $^3A_2(^3F)$ for $^{[4]}Ni^{2+}$ visible in absorption are marked by arrows and their superposition de- termines the complex shape of the absorption band. In contrast, as the emission is determined solely by the $^{[6]}Ni^{2+}$ species, the PL band has a nearly Gaussian shape.

5. Conclusions

A detailed spectroscopic study of the NiO-doped magnesium aluminosilicate glass nucleated by a mixture of TiO_2 and ZrO_2 during its heat-treatment has been performed and followed by an XRD analysis and Raman spectroscopy. *In situ* XRD measurements were applied to study the kinetics of crystal phase precipitation and to determine the crystallization sequence in detail. The initial glass was X-ray amorphous. According to XRD and Raman spectroscopy data, crystals of the nucleating catalyst, $ZrTiO_4$, about 4 nm in size, appear during the heat-treatment at 800°C; a small change in the Ni^{2+} environment is observed by absorption spectroscopy. There is no luminescence signal from the initial glass and glass heat-treated at 800°C. At 850°C, spinel crystals with size of about 6 nm precipitate. The $^{[5]}Ni^{2+}$ characteristic bands decrease rapidly in intensity due to the formation of the $^{[6]}Ni^{2+}$ species in Ni-doped spinel crystals, which is accompanied by a broadband luminescence in the near-IR centered at 1330 nm with FWHM of 380 nm. An

increase of the luminescence intensity after heat-treatment at 950°C is associated with an increase of volume fraction of Ni^{2+}- containing spinel nanophase and growth of individual nano-crystals. The increase of the luminescence intensity observed after additional low-temperature heat-treatment at 850°C is associated with a continuous growth of spinel volume fraction.

Acknowledgements

This work was partly supported by the RFBR (Grant 16-03- 01130). P.L. acknowledges financial support from the Government of the Russian Federation, Russia (Grant 074- U01) through ITMO Post-Doctoral Fellowship scheme. This work was supported in partby Russian Science Foundation (Agreement # 18-13-00200).

References

[1] L.F. Johnson, H.J. Guggenheim, D. Bahnck, A.M. Johnson, Phonon-terminated laser emission from Ni^{2+} ions in $KMgF_3$, Opt. Lett. 8 (1983) 371e373.

[2] W.E. Vehse, K.H. Lee, S.I. Yun, W.A. Sibley, Ni^{2+} emission in MgO, $KMgF_3$, $KZnF_3$ and MgF_2, J. Lumin. 10 (1975) 149e162.

[3] J.F. Donegan, G.P. Morgan, T.J. Glinn, G. Walker, New materials for tunable lasers in the near infrared, J. Mod. Opt. 4 (1990) 769e777.

[4] J.F. Donegan, F.J. Bergin, T.J. Glynn, G.F. Imbusch, The optical spectroscopy of $LiGa_5O_8$:Ni^{2+}, J. Lumin. 1 (1986) 57e63.

[5] C. Wyon, J.J. Aubert, F. Auzel, Czochralski growth and optical properties of magnesium-aluminum spinel doped with nickel, J. Cryst. Growth 79 (1986) 710e713.

[6] N.V. Kuleshov, V.G. Shcherbitsky, V.P. Mikhailov, S. Kuck, J. Koetke, K. Petermann, G. Huber, Spectroscopy and excited-state absorption of Ni^{2+}- doped $MgAl_2O_4$, J. Lumin. 71 (1997) 265e268.

[7] S. Kück, Laser-related spectroscopy of ion-doped crystals for tunable solid- state lasers, Appl. Phys. B 72 (2001) 515e562.

[8] A. Jouini, A. Yoshikawa, Y. Guyot, A. Brenier, T. Fukuda, G. Boulon, Potential candidate for new tunable solid-state laser between 1 and 2 mm: Ni^{2+}-doped $MgAl_2O_4$ spinel grown by the micro-pulling-down method, Opt. Mater. 30

(2007) 47e49.

[9] T. Suzuki, M. Hughes, Y. Ohishi, Optical properties of Ni-doped $MgGa_2O_4$ single crystals grown by floating zone method, J. Lumin. 130 (2010) 121e126.

[10] Q. Pan, S. Ye, D. Yang, J. Qiu, G. Dong, Multifunctional magnetic-fluorescent Ni-doped $ZnAl_2O_4$ nanoparticles with second biological NIR window fluores- cence, Mater. Res. Bull. 93 (2017) 310e317.

[11] S. Ye, Y. Zhang, H. He, J. Qiu, G. Dong, Simultaneous broadband near-infrared emission and magnetic properties of single phase Ni^{2+}-doped b-Ga_2O_3 nanocrystals via mediated phase-controlled synthesis, J. Mater. Chem. C 3

(2015) 2886e2896.

[12] J. Nie, Y. Li, S. Liu, Q. Chen, Q. Xu, J. Qiu, Tunable long persistent luminescence in the second near-infrared window via crystal field control, Sci. Rep. 7 (2017) 12392.

[13] J. Zheng, Y. Cheng, Z. Deng, Y. Xiong, Super broadband near-infrared lumi- nescence in Ni^{2+}-Er^{3+} co-doped transparent glass ceramics, J. Non-Cryst. Solids 471 (2017) 446e451.

[14] J. Cao, H. Guo, F. Hu, L. Li, S. Xu, M. Peng, Instant precipitation of $KMgF_3$:Ni^{2+} nanocrystals with broad emission (1.3-2.2 mm) for potential combustion gas

sensors, J. Am. Ceram. Soc. 101 (2018) 3890e3899.

[15] G.K.B. Costa, L.P. Sosman, A. Lypez, N. Cella, R.B. Barthem, Optical and struc- tural properties of Ni^{2+}-doped magnesium gallate polycrystalline samples, J. Alloys Compd. 534 (2012) 110e114.

[16] T. Bhasin, A. Agarwal, S. Sanghi, R.K. Kotnala, J. Shah, M. Yadav, M. Tuteja, Crystal structure, dielectric, magnetic and magnetoelectric properties of x$NiFe_2O_4$-(1-x)$Na_{0.5}Bi_{0.5}TiO_3$ composites, J. Alloys Compd. 748 (2018) 1022e1030.

[17] S. Kumar, D.P. Dubey, S. Shannigrahi, R. Chatterjee, Complex permittivity, permeability, magnetic and microwave absorbing properties of Ni^{2+} substituted mechanically milled U-type hexaferrites, J. Alloys Compd. 774 (2019) 52e60.

[18] T. Amjad, I. Sadiq, A.B. Javaid, S. Riaz, S. Naseem, M. Nadeem, Investigation of structural, electrical, electrical polarization and dielectric properties of CTAB assisted Ni^{2+} substituted R-type nano-hexaferrites, J. Alloys Compd. 770

(2019) 1112e1118.

[19] Y.A. Alsabah, M.S. AlSalhi, A.A. Elbadawi, E.M. Mustafa, Influence of Zn^{2+} and Ni^{2+} cations on the structural and optical properties of $Ba_2Zn_{1-x}Ni_xWO_6$ ($0 \leq x \leq 1$) tungsten double perovskites, J. Alloys Compd. 701 (2017) 797e805.

[20] L.R. Pinckney, G.H. Beall, Transition element-doped crystals in glass, Proc. SPIE 4452 (2001) 93e99.

[21] B.N. Samson, L.R. Pinckney, J. Wang, G.H. Beall, N.F. Borrelli, Nickel-doped nanocrystalline glass-ceramic fiber, Opt. Lett. 15 (2002) 1309e1311.

[22] T. Suzuki, K. Horibuchi, Y. Ohishi, Structural and optical properties of ZnO-eAl_2O_3eSiO_2 system glasseceramics containing Ni^{2+}-doped nanocrystals, J. Non-Cryst. Solids 351 (2005) 2304e2309.

[23] T. Suzuki, G.S. Murugan, Y. Ohishi, Optical properties of transparent Li_2O- Ga_2O_3-SiO_2 glass-ceramics embedding Ni-doped nanocrystals, Appl. Phys. Lett. 86 (2005), 131903, 1-3.

[24] T. Suzuki, Y. Arai, Y. Ohishi, Quantum efficiencies of near-infrared emission from Ni^{2+}-doped glass-ceramics, J. Lumin. 128 (2008) 603e609.

[25] B. Wu, S. Zhou, J. Qiu, M. Peng, L. Yang, X. Jiang, C. Zhu, Transparent Ni^{2+}-

doped MgOeAl_2O_3eSiO_2 glass ceramics with broadband infrared lumines- cence, Chin. Phys. Lett. 23 (2006) 2778e2781.

[26] B. Wu, J. Qiu, M. Peng, J. Ren, X. Jiang, C. Zhu, Transparent Ni^{2+}-doped ZnO-

Al_2O_3-SiO_2 system glass-ceramics with broadband infrared luminescence, Mater. Res. Bull. 42 (2007) 762e768.

[27] B. Wu, N. Jiang, S. Zhou, D. Chen, C. Zhu, J. Qiu, Transparent Ni^{2+}-doped silicate

glass ceramics for broadband near-infrared emission, Opt. Mater. 30 (2008) 1900e1904.

[28] S. Zhou, N. Jiang, K. Miura, S. Tanabe, M. Shimizu, M. Sakakura, Y. Shimotsuma,

M. Nishi, J. Qiu, K. Hirao, Simultaneous tailoring of phase evolution and dopant distribution in the glassy phase for controllable luminescence, J. Am. Chem. Soc. 132 (2010) 17945e17952.

[29] S. Zhou, J. Hao, J. Qiu, Ultra-broadband near-infrared luminescence of Ni^{2+}:

$ZnOeAl_2O_3eSiO_2$ nanocomposite glasses prepared by solegel method, J. Am. Ceram. Soc. 9 (2011) 2902e2905.

[30] V.N. Sigaev, N.V. Golubev, E.S. Ignat'eva, V.I. Savinkov, M. Campione,

R. Lorenzi, F. Meinardi, A. Paleari, Nickel-assisted growth and selective doping of spinel-like gallium oxide nanocrystals in germano-silicate glasses for infrared broadband light emission, Nanotechnology 23 (2012), 015708, 1-7.

[31] J. Qiu, Controlling the metastable states of glasses by external fields, J. Appl. Glass Sci. 7 (2016) 270e284.

[32] G. Bai, J. Hao, Novel metal ion doped photonic materials with ultrabroadband near-infrared luminescence, Sci. Adv. Today 2 (2016) 25228.

[33] P.A. Loiko, O.S. Dymshits, A.A. Zhilin, I.P. Alekseeva, K.V. Yumashev, Influence of NiO on phase transformations and optical properties of ZnO-Al_2O_3-SiO_2 glass-ceramics nucleated by TiO_2 and ZrO_2. Part II. Optical absorption and luminescence, J. Non-Cryst. Solids 376 (2013) 99e105.

[34] Z. Gao, Y. Liu, J. Ren, Z. Fang, X. Lu, E. Lewis, G. Farrell, J. Yang, P. Wang, Se- lective doping of Ni^{2+} in highly transparent glass-ceramics containing nano- spinels $ZnGa_2O_4$ and $Zn_{1+x}Ga_{2-2x}Ge_xO_4$ for broadband near-infrared fiber ampli ers, Sci. Rep. 7 (2017) 1783, 1-8.

[35] Z. Gao, X. Lu, Y. Zhang, S. Guo, L. Liu, G. Yang, Y. Liu, S. Sun, J. Ren, J. Yang, Correlation between ultrabroadband near-infrared emission and Yb^{3+}/Ni^{2+} dopants distribution in highly transparent germanate glass ceramics con-

taining zinc gallogermanate nanospinels, J. Am. Ceram. Soc. (2018), https:// doi.org/10.1111/jace.16028.

[36] X. Liu, J. Zhou, S. Zhou, Y. Yue, J. Qiu, Transparent glass-ceramics functional- ized by dispersed crystals, Prog. Mater. Sci. 97 (2018) 38e96.

[37] Z. Gao, S. Guo, X. Lu, J. Orava, T. Wagner, L. Zheng, Y. Liu, S. Sun, F. He, P. Yang,

J. Ren, J. Yang, Controlling selective doping and energy transfer between transition metal and rare earth ions in nanostructured glassy solids, Adv. Opt. Mater. (2018), 1701407, 1-9.

[38] D.M. Roy, R. Roy, E.F. Osborn, The system $MgO-Al_2O_3-H_2O$ and influence of carbonate and nitrate ions on the phase equilibria, Am. J. Sci. 251 (1953) 337e361.

[39] A. Navrotsky, B.A. Wechsler, K. Geisinger, F. Seifert, Thermochemistry of $MgAl_2O_4$-$Al_{8/3}O_4$ defect spinels, J. Am. Ceram. Soc. 69 (1986) 418e422.

[40] S. Pal, A.K. Bandyopadhyay, S. Mukherjee, B.N. Samaddar, P.G. Pay, $MgAl_2O_4$eg-Al_2O_3 solid solution interaction: mathematical framework and phase separation of a-Al_2O_3 at high temperature, Bull. Mater. Sci. 34 (2011) 859e864.

[41] Y. Suwa, R. Roy, S. Komarneni, Lowering the sintering temperature and enhancing densification by epitaxy in structurally diphasic Al_2O_3 and Al_2O_3- MgO xerogels, Mater. Sci. Eng. 83 (1986) 151e159.

[42] A. Navrotsky, O.J. Kleppa, The thermodynamics of cation distributions in simple spinels, J. Inorg. Nucl. Chem. 29 (1967) 270le2714.

[43] B.J. Wood, R.J. Kirkpatrick, B. Montez, Order-disorder phenomena in $MgAl_2O_4$ spinel, Am. Mineral. 71 (1986) 999e1006.

[44] P. Porta, F.S. Stone, R.G. Turner, The distribution of nickel ions among octa- hedral and tetrahedral sites in $NiAl_2O_4$-$MgAl_2O_4$ solid solutions, J. Solid State Chem. 11 (1974) 135e147.

[45] I.P. Alekseeva, O.S. Dymshits, V.V. Golubkov, P.A. Loiko, M.Ya. Tsenter,

K.V. Yumashev, S.S. Zapalova, A.A. Zhilin, Influence of NiO on phase trans- formations and optical properties of $ZnOeAl_2O_3eSiO_2$ glass-ceramics nucle- ated by TiO_2 and ZrO_2. Part I. Influence of NiO on phase transformations of $ZnOeAl_2O_3eSiO_2$ glass-ceramics nucleated by TiO_2 and ZrO_2, J. Non-Cryst. Solids 384 (2014) 73e82.

[46] A. Dugué, O. Dymshits, L. Cormier, B. Cochain, G. Lelong, A. Zhilin, S. Belin, *In situ* evolution of Ni environment in magnesium aluminosilicate glasses and glasseceramicseInfluence of ZrO_2 and TiO_2 nucleating agents, J. Phys. Chem. Solids 78 (2015) 137e146.

[47] T. Degen, M. Sadki, E. Bron, U. Kœnig, G. Nénert, The high Score suite, Powder Diffr. 29 (Suppl. S2) (December 2014) S13eS18.

[48] H. Lipson, H. Steeple, in: McMillan (Ed.), Interpretation of X-ray Powder Patterns, Martins Press, London, N.Y., 1970.

[49] B. Cochain, L. Cormier, A. Novikova, G. Lelong, S. Belin, X.H. Zhang, Insitu local environment and partitioning of Ni^{2+} ions during crystallization of an oxy- fluoride glass, J. Non-Cryst. Solids 408 (2015) 7e12.

[50] J. Xu, C. Lind, A.P. Wilkinson, S. Pattanaik, X-ray diffraction and X-ray ab- sorption spectroscopy studies of sol-gel-processed zirconium titanates, Chem. Mater. 12 (2000) 3347e3355.

[51] G. Carl, T. Hœche, B. Voigt, Crystallization behaviour of a MgO-

$eAl_2O_3eSiO_2eTiO_2eZrO_2$ glass, Phys. Chem. Glasses 43C (2002) 256e258.

[52] A. Ono, Solid solutions in the system ZrO_2-TiO_2, Mineral. J. 6 (1972) 433e441.

[53] Troitzsch, A.G. Christy, D.J. Ellis, The crystal structure of disordered $(Zr,Ti)O_2$ solid solution including srilankite: evolution towards tetragonal ZrO_2 with increasing Zr, Phys. Chem. Miner. 32 (2005) 504e514.

[54] T.I. Chuvaeva, O.S. Dymshits, V.I. Petrov, M.Ya. Tsenter, A.V. Shashkin,

A.A. Zhilin, V.V. Golubkov, Low-frequency Raman scattering of magnesium aluminosilicate glasses and glass-ceramics, J. Non-Cryst. Solids 282 (2001) 306e316.

[55] P. McMillan, B. Piriou, A. Navrotsky, A Raman spectroscopic study of glasses along the joins silica-calcium aluminate, silica-sodium aluminate, and silica- potassium aluminate, Geochim. Cosmochim. Acta 46 (1982) 2021e2037.

[56] G. Henderson, D. Neuville, R. Downs, Advances in Raman spectroscopy applied to earth and material sciences, Rev. Mineral. Geochem. 78 (2014) 509e541.

[57] D.R. Neuville, L. Cormier, V. Montouillout, P. Florian, F. Millot, J.-C. Rifflet,

D. Massiot, Structure of Mg- and Mg/Ca aluminosilicate glasses: ^{27}Al NMR and Raman spectroscopy investigations, Am. Mineral. 93 (2008) 1721e1731.

[58] I. Alekseeva, O. Dymshits, 1 V. Golubkov, A. Shashkin, M. Tsenter, A. Zhilin, Phase transformations in NiO and CoO doped magnesium aluminosilicate glasses nucleated by ZrO_2, Glass Technol. 46 (2005) 187e191.

[59] V. Keramidas, W.B. White, Raman scattering study of the crystallization and phase transformations of ZrO_2, J. Am. Ceram. Soc. 57 (1974) 22e24.

[60] L.G. Karakhiev, E.G. Avvakumov, O.B. Vinokurova, A.A. Gusev, N.Z. Lyakhov, Soft mechanochemical synthesis of dispersed zirconium titanate, Chem. Sustain. Dev. 3 (2003) 483e487.

[61] Ya.S. Bobovich, Spectroscopy of titanium coordination states in some vitreous materials, Opt. Spektrosk. 14 (1963) 647e654.

[62] B.G. Varshal, A.V. Bobrov, B.N. Mavrin, V.V. Iljukhin, N.V. Belov, DAN USSR 216 (1974) 374e377.

[63] S. Sakka, F. Miyaji, K. Fukumi, Structure of binary K_2O-TiO_2 and Cs_2O-TiO_2 glasses, J. Non-Cryst. Solids 112 (1989) 64e68.

[64] G.S. Henderson, M.E. Fleet, The structure of Ti silicate glasses by microRaman spectroscopy, Can. Mineral. 33 (1995) 399e408.

[65] M.A. Krebs, R.A. Condrate Sr., A Raman spectral characterization of various crystalline mixtures in ZrO_2 - TiO_2 and HfO_2 - TiO_2 systems, J. Mater. Sci. Lett. 7 (1988) 1327e1330.

[66] F. Azough, R. Freer, J. Petzelt, A Raman spectral characterization of ceramics in the system ZrO_2eTiO_2, J. Mater. Sci. 28 (1993) 2273.

[67] Y.K. Kim, H.M. Jang, Lattice contraction and cation ordering of $ZrTiO_4$ in the normal-to-incommensurate phase transition, J. Appl. Phys. 89 (2001) 6349e6355.

[68] P.R. de Lucena, E.R. Leite, F.M. Pontes, E. Longo, P.S. Pizani, J.A. Varela, Photoluminescence: a probe for short, medium and long-range self-organization order in $ZrTiO_4$ oxide, J. Solid State Chem. 179 (2006) 3997e4002.

[69] P.F. McMillan, Structural studies of silicate glasses and melts - applications and limitations of Raman spectroscopy, Am. Mineral. 69 (1984) 622e644.

[70] M.P. O'Horo, A.L. Frisillo, W.B. White, Lattice vibrations of $MgAl_2O_4$ spinel,

J. Phys. Chem. Solids 34 (1973) 23e28.

[71] M. Ishii, J. Hiraishi, T. Yamanaka, Structure and lattice vibrations of Mg-Al spinel solid solution, Phys. Chem. Miner. 8 (1982) 64e68.

[72] H. Cynn, S.J. Sharma, T.F. Cooney, M. Nicol, High-temperature Raman investigation of order-disorder behaviour in the $MgAl_2O_4$ spinel, Phys. Rev. B 45 (1992) 500e502.

[73] I. Alekseeva, A. Baranov, O. Dymshits, V. Ermakov, V. Golubkov, M. Tsenter,

A. Zhilin, Influence of CoO addition on phase separation and crystallization of glasses of the $ZnOeAl_2O_3eSiO_2eTiO_2$ system, J. Non-Cryst. Solids 357 (2011) 3928e3939.

[74] L. Galoisy, G. Calas, Structural environment of nickel in silicate glass/melt systems: Part 1 Spectroscopic determination of coordination states, Geochim. Cosmochim. Acta 57 (1993) 3613e3626.

[75] R.D. Tchana, T. Pfeiffer, B. Rüdinger, J. Deubener, Spectroscopy study on the nucleation kinetics of $ZrTiO_4$ in a lithium alumosilicate glass, J. Non-Cryst. Solids 384 (2014) 25e31.

[76] M. Dondi, F. Matteucci, G. Cruciani, Zirconium titanate ceramic pigments: crystal structure, optical spectroscopy and technological properties, J. Solid State Chem. 179 (2006) 233e246.

[77] S. Lin, X. Zhang, P. Zhang, D. Tan, J. Xu, W. Li, K. Chen, High-efficiency near-infrared emission from Bismuth-doped $SiO_{0.73}$ thin films fabricated by ion implantation technology, Opt. Lett. 41 (2016) 630e633.

[78] V.V. Golubkov, O.S. Dymshits, A.A. Zhilin, T.I. Chuvaeva, A.V. Shashkin, The Influence of nickel oxide additives on the phase separation and crystallization of glasses in the $MgOeAl_2O_3eSiO_2eTiO_2$ system, Glass Phys. Chem. 30 (2004) 300e310.

[79] X. Zhang, P. Wang, D. Qi, Y. Huang, B. Zheng, T. Lin, P. Chen, Z. Yu, J. Xu, Enhanced and wavelength-tunable near-infrared luminescence from bismuth-doped silica thin films with Au nanocrystals, J. Alloys Compd. 772 (2019) 332e336.